Peer-Reviewed Technical Communication

Instantaneous Global Navigation Satellite System (GNSS)-Based Attitude Determination for Maritime Applications

Gabriele Giorgi, Peter J. G. Teunissen, *Member, IEEE*, and Tim P. Gourlay

***Abstract*—Global Navigation Satellite System (GNSS) is a valuable technology for a large number of maritime applications. Other than providing the absolute positioning service, it aids many demanding applications, such as precise docking, formation of surface craft, autonomous vehicles, sinkage monitoring, etc. GNSS carrier-phase-based algorithms provide high-precision positioning solutions, but an integer number of cycles inherent to the observed signal have to be resolved. A newly developed GNSS carrier-phase ambiguity resolution method is tested. The new method solves for the unknown number of integer cycles by exploiting the known placement of the GNSS antennas aboard the vessel. The *a priori* information on the antennas baseline separation is employed as a hard constraint. A simplified (linearized) version of the method, suitable for large vessels, is also analyzed. The new method was tested against the most challenging scenario when processing GNSS data: single-frequency, single-epoch, unaided ambiguity resolution. Through different tests, the high performance of the new method is demonstrated: high fixing rate, large robustness, and short time-to-fix after initialization, cycle slips, and/or loss of locks. Considerations about the wide spectra of maritime applications are given, and a specific experiment is carried out to demonstrate the capabilities of the method for navigation in shallow waters.**

***Index Terms*—Ambiguity resolution, constrained least squares, Global Navigation Satellite System (GNSS), shipborne attitude, sinkage monitoring, under-keel clearance (UKC).**

I. Introduction

GLOBAL NAVIGATION SATELLITE SYSTEM (GNSS) technology is currently an essential instrument for maritime applications. The global satellite coverage provides a precise and timely absolute positioning service in any given place on the globe. Very accurate real-time kinematic (RTK) solutions are used for applications such as precise docking [1]–[3], under-keel clearance (UKC), dynamic draught estimations [4], [5], guidance of autonomous surface vehicles (ASVs) [6], formation control [7], attitude estimation [8]–[10], guidance in shallow waters [11], etc.

High-precision GNSS-based applications make use of the carrier-phase measurements. Next to the GNSS code signal, the fractional part of the incoming GNSS signal phase is also stored as an observable. However, the phase measurements are ambiguous by an unknown numbers of whole cycles, which have to be resolved to significantly augment the precision of the range estimation. Carrier-phase integer ambiguity resolution is the key toward precise GNSS-based estimations of a ship's (relative) position and attitude. The task of resolving the ambiguities as integers is nontrivial, especially if one aims at reliable and fast techniques, ideally capable of providing instantaneous (i.e., based on single epoch of data) correct estimations. Various methods that differ in the way the problem is approached and solved (see, for further discussion, [12]–[14] and references therein) have been proposed in literature. This contribution focuses on the integer least squares (ILS) principle [15] that applies to linear systems where a subset of the unknowns is integer valued. A well-known implementation of the ILS principle is the Least-squares AMBiguity Decorrelation Adjustment (LAMBDA) method [16], a widely used ambiguity resolution algorithm for unconstrained and linearly constrained applications [17]–[21]. Although very effective, the method is not specifically designed for nonlinear constrained applications, such as GNSS-based attitude determination, where multiantenna frames of known geometry are employed. The algorithm tested in this contribution is an extension of the LAMBDA method, modified to rigorously incorporate the *a priori* information on the antennas baseline separation.

By providing superior performance in terms of capacity of fixing the correct set of integer ambiguities in a timely manner, the baseline constrained LAMBDA (C-LAMBDA) method brings numerous advantages. It avoids the use of multiple high grade antennas/receivers to be placed aboard the ship to reliably estimate its attitude; it provides a robust baseline solution in the shortest time; it does not rely on any *a priori* information from different sensors or dynamic model; and it is independent from the platform dynamic.

The method is extensively tested on data collected on a vessel sailing into a small canal in The Netherlands and on large container ships approaching the harbor of Hong Kong. The accuracy of the solution is investigated with a static test, where the

Manuscript received September 01, 2010; revised February 13, 2012; accepted March 19, 2012. Date of publication May 16, 2012; date of current version July 10, 2012. The work of P. J. G. Teunissen was supported by an Australian Research Council Federation Fellowship (Project FF0883188).

Associate Editor: W. M. Carey.

G. Giorgi is with the Institute for Communications and Navigation, Technische Universität München, Munich D-80333, Germany (e-mail: gabriele.giorgi@tum.de).

P. J. G. Teunissen is with the Department of Spatial Sciences, Curtin University of Technology, Perth, W.A. 6845, Australia and the Department of Earth Observation and Satellite Systems, Delft University of Technology, Delft 2629, The Netherlands (e-mail: p.teunissen@curtin.edu.au).

T. P. Gourlay is with the Centre for Marine Science and Technology, Curtin University of Technology, Perth, W.A. 6845, Australia (e-mail: t.gourlay@cmst.curtin.edu.au).

Color versions of one or more of the figures in this paper are available online at http://ieeexplore.ieee.org.

Digital Object Identifier 10.1109/JOE.2012.2191996

influence of the baseline length on the final attitude solution is also given.

II. The Constrained Model for the GNSS Observations

Assume to track $n+1$ GNSS satellites at two points (antennas) aboard a ship. The raw GNSS carrier-phase and code observations collected at each antenna are first differenced between them [single differences (SDs)], then differenced between two given satellites [double differences (DDs)]. The differencing operation cancels out the receiver and satellite clock errors and delays [22]. Furthermore, if the distance between the antennas is shorter than a few hundred meters, the difference between the atmospheric delays becomes negligible [22]. The resulting DD observations (tracking N frequencies) are cast with the linear(ized) system

$$\begin{aligned} &E(y) = Aa + Bb \\ &D(y) = Q_{yy}, \qquad a \in \mathbb{Z}^{Nn}, \qquad b \in \mathbb{R}^3, \qquad \|b\| = l \end{aligned} \tag{1}$$

with $E(\cdot)$ and $D(\cdot)$ the expectation and dispersion operator, respectively. The vector y (order $2Nn$) collects the DD phase and code observations, whose dispersion is described by the positive-definite variance–covariance (v–c) matrix Q_{yy}. The unknowns are the Nn integer ambiguities in a and the real-valued baseline coordinates b. The antennas are assumed to be separated by the known baseline length l: this constrains the baseline coordinates. A and B are the design matrices, obtained as follows:

$$\begin{aligned} &\text{single frequency: } A = \begin{bmatrix} \mathbf{0} \\ \lambda_{L_1} I_n \end{bmatrix}, \quad B = \begin{bmatrix} G \\ G \end{bmatrix} \\ &\text{dual frequency: } A = \begin{bmatrix} \mathbf{0} & \\ \lambda_{L_1} I_n & \\ & \mathbf{0} \\ & \lambda_{L_2} I_n \end{bmatrix}, \quad B = \begin{bmatrix} G \\ G \\ G \\ G \end{bmatrix}, \\ &G = \begin{bmatrix} (-u^1)^T \\ \vdots \\ (-u^n)^T \end{bmatrix} \end{aligned} \tag{2}$$

where λ_i is the carrier wavelength at frequency i. The rows of matrix G correspond to the line-of-sight vectors u^i. The least squares solution of system (1) follows from minimizing the squared weighted norm

$$\min_{a \in \mathbb{Z}^{Nn}, b \in \mathbb{R}^3, \|b\| = l} \|y - Aa - Bb\|^2_{Q_{yy}} \tag{3}$$

with $\|\cdot\|^2_Q = (\cdot)^T Q^{-1} (\cdot)$. Solving (3) is nontrivial, due to the distinct nature of the constraints on the vectors of unknowns a and b. Disregarding only the baselines length constraint, the model is solved by applying the ILS principle [15]. Keeping the nonlinear constraint on b, but disregarding the integer nature of the ambiguities, makes (3) a constrained least squares problem, for which many solutions are available (such as iterative algorithms like the Gauss–Newton and the Newton methods, or techniques based on the singular value decomposition (SVD) [23]). Considering both constraints in an integral solution requires a nontrivial modification of the discrete search strategy necessary to apply the ILS principle, which has to accommodate the additional nonlinear geometrical constraint. In the next sections, different solutions of the ambiguity resolution problem are reviewed and tested. It is stressed that the constrained solution is given only for the single-frequency case $(N = 1)$.

A. The Baseline Unconstrained Solution

Disregarding the baseline constraint in (3), the minimization problem is formulated as

$$\min_{a \in \mathbb{Z}^{Nn}, b \in \mathbb{R}^3} \|y - Aa - Bb\|^2_{Q_{yy}}. \tag{4}$$

Among the different solutions available to approach this integer minimization problem, the LAMBDA method is widely used for its efficiency and quickness.

Three steps are necessary to extract the ILS minimizer of (4): derive the float solution, search the integer minimizer, and adjust the baseline solution according to the resolved integer ambiguities.

First, the float solution of (4), without considering any constraint (so that $\hat{a} \in \mathbb{R}^{Nn}, \hat{b} \in \mathbb{R}^3$), is obtained by applying the (weighted) least squares principle

$$\begin{bmatrix} A^T Q_{yy}^{-1} A & A^T Q_{yy}^{-1} B \\ B^T Q_{yy}^{-1} A & B^T Q_{yy}^{-1} B \end{bmatrix} \begin{pmatrix} \hat{a} \\ \hat{b} \end{pmatrix} = \begin{bmatrix} A^T Q_{yy}^{-1} \\ B^T Q_{yy}^{-1} \end{bmatrix} y. \tag{5}$$

The v–c matrices of the float solution $Q_{\hat{a}\hat{a}}$, $Q_{\hat{a}\hat{b}}$, and $Q_{\hat{b}\hat{b}}$ are obtained as

$$\begin{bmatrix} Q_{\hat{a}\hat{a}} & Q_{\hat{a}\hat{b}} \\ Q_{\hat{b}\hat{a}} & Q_{\hat{b}\hat{b}} \end{bmatrix} = \begin{bmatrix} A^T Q_{yy}^{-1} A & A^T Q_{yy}^{-1} B \\ B^T Q_{yy}^{-1} A & B^T Q_{yy}^{-1} B \end{bmatrix}^{-1}. \tag{6}$$

Assuming the integer ambiguities a as known, the (fixed) baseline coordinates can be found by solving the system $E(y - Aa) = Bb$, $D(y) = Q_{yy}$. The fixed vector $\hat{b}(a)$ is related to the float solution $\hat{b}$ as

$$\hat{b}(a) = \left(B^T Q_{yy}^{-1} B\right)^{-1} B^T Q_{yy}^{-1} (y - Aa) = \hat{b} - Q_{\hat{b}\hat{a}} Q_{\hat{a}\hat{a}}^{-1} (\hat{a} - a) \tag{7}$$

with corresponding v–c matrix

$$Q_{\hat{b}(a)\hat{b}(a)} = Q_{\hat{b}\hat{b}} - Q_{\hat{b}\hat{a}} Q_{\hat{a}\hat{a}}^{-1} Q_{\hat{a}\hat{b}}. \tag{8}$$

The precision of the adjusted baseline vector $\hat{b}(a)$ is considerably higher than the precision of the float solution $\hat{b}$: the entries of $Q_{\hat{b}(a)\hat{b}(a)}$ are driven by the accuracy of the phase observables that are of two orders of magnitude more precise than the code measurements [22].

The following step takes into account the integer nature of the carrier-phase ambiguities: $a \in \mathbb{Z}^{Nn}$. The minimization problem (4) can be decomposed as a sum of squares [22]

$$\begin{aligned} &\min_{a \in \mathbb{Z}^{Nn}, b \in \mathbb{R}^3} \|y - Aa - Bb\|^2_{Q_{yy}} \\ &= \min_{a \in \mathbb{Z}^{Nn}, b \in \mathbb{R}^3} \left(\|\hat{e}\|^2_{Q_{yy}} + \|\hat{a} - a\|^2_{Q_{\hat{a}\hat{a}}} + \left\| \hat{b}(a) - b \right\|^2_{Q_{\hat{b}(a)\hat{b}(a)}} \right) \end{aligned} \tag{9}$$

where $\hat{e}$ is the vector of residuals. Without considering the constraint on the baseline vector, the last term on the right-hand

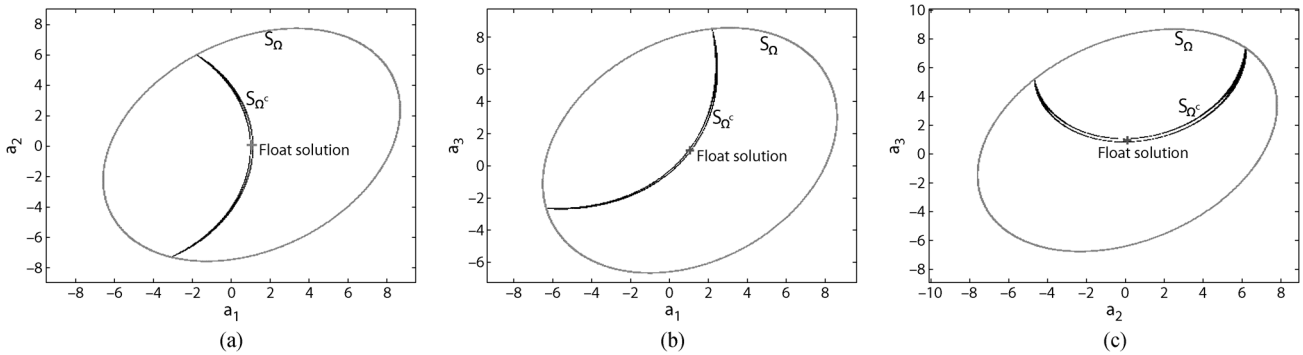

Fig. 1. "Slices" of the contour surfaces $\mathbb{S}_{\Omega}(\chi^2) = \{a \in \mathbb{R}^n | \|\hat{a} - a\|^2_{Q_{\hat{a}\hat{a}}} - \chi^2 | \leq \epsilon\}$ and $\mathbb{S}_{\Omega^C}(\chi^2) = \{a \in \mathbb{R}^n | |C(a) - \chi^2| \leq \epsilon\}$, with ϵ sufficiently small. Each slice contains the float solution (center of the ellipsoidal search space). (a) Section 1 and 2 of the search spaces Ω and Ω^C. (b) Section 1–3 of the search spaces Ω and Ω^C. (c) Section 2 and 3 of the search spaces Ω and Ω^C.

side can be made zero for any choice of a. The minimization problem then reduces to

$$\check{a} = \arg \min_{a \in \mathbb{Z}^{Nn}} \|\hat{a} - a\|^2_{Q_{\hat{a}\hat{a}}}. \tag{10}$$

Closed-from solutions of (10) do not exist: the minimization implies a discrete search strategy in an admissible set of integer candidates (the search space) defined as

$$\Omega(\chi^2) = \left\{a \in \mathbb{Z}^{Nn} | \|\hat{a} - a\|^2_{Q_{\hat{a}\hat{a}}} \leq \chi^2\right\}. \tag{11}$$

The search space is an ellipsoid, centered in $\hat{a}$ and whose shape is driven by the v–c matrix $Q_{\hat{a}\hat{a}}$. The size of the set is limited by the scalar χ, whose choice is fundamental: it has to be small enough to limit the computational load, but large enough to guarantee the nonemptiness of the set. It is demonstrated in practice that bootstrapping a solution $\acute{a}$ with weight matrix $Q^{-1}_{\hat{a}\hat{a}}$ provides a good choice for the initial size of the search space: $\chi^2_0 = \|\hat{a} - \acute{a}\|^2_{Q_{\hat{a}\hat{a}}}$. The ambiguity search space (11) usually has a significant elongation due to the covariance properties of the double differenced ambiguities [22], which are highly correlated. This results in an inefficient search for the integer minimizer. The LAMBDA method overtakes the problem by means of a decorrelation of the v–c matrix $Q_{\hat{a}\hat{a}}$ that smooths the covariance spectrum, achieved by a linear transformation that preserves the integer nature of the parameters. As a result, the search becomes much faster in the decorrelated space and the computation of the integer minimizer is performed in a timely manner.

The conclusive step is to adjust the float baseline vector according to the extracted integer minimizer $\check{a}$

$$\check{b} = \hat{b}(\check{a}) = \hat{b} - Q_{\hat{b}\hat{a}} Q^{-1}_{\hat{a}\hat{a}} (\hat{a} - \check{a}). \tag{12}$$

B. The Baselines Constrained Solution

For frames of antennas mounted on the same rigid body, the baseline separation is employed as a hard constraint. This strengthens the observation model, improving the performance of the ambiguity estimation. The additional constraint is used both in the derivation of the float solution and, most importantly, in driving the ambiguity search. Since the additional *a priori* information is used to strengthen the underlying model, the constrained solution is presented only for the weaker single-frequency model $(N = 1)$.

The unconstrained float solutions $\hat{a}$ and $\hat{b}$ are derived according to (5). By using the same sum-of-squares decomposition given in (9), the minimization problem now reads

$$\begin{aligned} \check{a} &= \arg \min_{a \in \mathbb{Z}^n} C(a) \\ &= \arg \min_{a \in \mathbb{Z}^n} \left(\|\hat{a} - a\|^2_{Q_{\hat{a}\hat{a}}} + \left\|\hat{b}(a) - \check{b}(a)\right\|^2_{Q_{\hat{b}(a)\hat{b}(a)}} \right) \\ \check{b}(a) &= \arg \min_{b \in \mathbb{R}^3, \|b\| = l} \left\|\hat{b}(a) - b\right\|^2_{Q_{\hat{b}(a)\hat{b}(a)}}. \end{aligned} \tag{13}$$

Note that the ambiguity objective function has become nonquadratic in a due to the presence of the second term. Other ambiguity objective functions have been used in the literature. However, none of these have the nonlinear constraints rigorously incorporated into the ambiguity objective function. For a comparison and discussion, we refer to [14].

The baseline term in (13) can no longer be made zero for any choice of a, and its evaluation is necessary to the computation of the cost function. The whole minimization process is complicated by the coupling of the two terms in (13). The evaluation of the cost function $C(a)$ requires the solution of a constrained least squares problem to extract the term $\check{b}(a)$, adding computational load for each integer candidate [14]. The set wherein the ambiguities are searched is no longer ellipsoidal

$$\Omega^C(\chi^2) = \left\{a \in \mathbb{Z}^n | C(a) \leq \chi^2\right\}. \tag{14}$$

Fig. 1 shows the search spaces $\Omega(\chi^2)$ and $\Omega^C(\chi^2)$ for a simulated four-satellites scenario, after the decorrelation of the ambiguities. The three sections of the 3-D contour surfaces are shown: these sections are "slices" of the contour surfaces $\mathbb{S}_{\Omega}(\chi^2) = \{a \in \mathbb{R}^n | \|\hat{a} - a\|^2_{Q_{\hat{a}\hat{a}}} - \chi^2| \leq \epsilon\}$ and $\mathbb{S}_{\Omega^C}(\chi^2) = \{a \in \mathbb{R}^n | |C(a) - \chi^2| \leq \epsilon\}$, with ϵ sufficiently small. Each slice contains the float solution (center of the ellipsoidal search space). The nonellipsoidal search space $\Omega^C(\chi^2)$ is moon shaped, and it contains much less candidates for the same χ.

Fig. 1 also visualizes a problem that arises with the constrained solution. Given a scalar χ for which the set $\Omega(\chi^2)$ is nonempty, the extensive evaluation of the set $\Omega^C(\chi^2)$ is highly inefficient: for many integer vectors, the cost function $C(a)$

might be unnecessarily computed. Moreover, the set $\Omega^C(\chi^2)$ might even turn out to be empty. The reason is that the second term $\|\hat{b}(a)-\check{b}(a)\|^2_{Q_{\hat{b}(a)\hat{b}(a)}}$ largely amplifies the value of $\chi^2 = C(\grave{a})$ for integer vectors $\acute{a}$ that provide a too large distance, in the metric of $Q_{\hat{b}(a)\hat{b}(a)}$, between $\hat{b}(\grave{a})$ and $\check{b}(\grave{a})$. Setting the value of χ^2 to guarantee the nonemptiness of the search space proves to be nontrivial, especially for those cases where the set of GNSS observations lacks sufficient strength, i.e., reduced number of available satellites, single frequency.

The C-LAMBDA method [24] has been designed to efficiently solve for (13). The search is made faster via the introduction of novel search techniques as the *search-and-shrink* approach [10], [14], [25], [26] or the *expansion* approach [13], [26], [27]. These search algorithms adaptively adjust the size of the search space by shrinking or expanding the set of candidates as the search proceeds, working with functions that are faster to evaluate than $C(a)$.

The two search strategies are based on the following property: the norm $\|\hat{b}(a)-b\|^2_{Q_{\hat{b}(a)\hat{b}(a)}}$ is bounded via the smallest (λ_m) and largest (λ_M) eigenvalues of the matrix $Q^{-1}_{\hat{b}(a)\hat{b}(a)}$ as

$$\begin{aligned} C_1(a) &= \|\hat{a}-a\|^2_{Q_{\hat{a}\hat{a}}} + \lambda_m \left(\left\| \hat{b}(a) \right\|^2_{I_3} - l \right)^2 \\ C_2(a) &= \|\hat{a}-a\|^2_{Q_{\hat{a}\hat{a}}} + \lambda_M \left(\left\| \hat{b}(a) \right\|^2_{I_3} - l \right)^2 \end{aligned} \tag{15}$$

with $C_1(a) \le C(a) \le C_2(a)$. The *expansion* approach works by enumerating all the integer vectors contained in a small set of admissible candidates

$$\Omega_1\left(\chi_0^2\right) = \left\{ a \in \mathbb{Z}^n | C_1(a) \le \chi_0^2 \right\} \supseteq \Omega^C\left(\chi_0^2\right) \tag{16}$$

where the scalar χ_0 is initially chosen small enough and iteratively increased until, at step s, the set $\Omega_1(\chi_s^2)$ turns out to be nonempty. As the evaluation of $C_1(a)$ only involves the computation of two squared norms, the enumeration proceeds rather quickly. For each of the enumerated integer vectors in $\Omega_1(\chi_s^2)$, the constrained least squares problem in (13) is solved and the set $\Omega^C(\chi_s^2)$ is evaluated: if it is empty, the scalar χ_s is increased to $\chi_{s+1} > \chi_s$ and the enumeration in $\Omega_1(\chi_{s+1}^2)$ repeated, otherwise the minimizer of $C(a)$ is picked up.

The *search-and-shrink* approach works in the opposite way. The search space relative to the bounding function $C_2(a)$ is defined as

$$\Omega_2\left(\chi_0^2\right) = \left\{ a \in \mathbb{Z}^n | C_2(a) \le \chi_0^2 \right\} \subseteq \Omega^C\left(\chi_0^2\right) \tag{17}$$

where χ_0 is chosen large enough to guarantee the nonemptiness of $\Omega_2(\chi_0^2)$. The search proceeds by iteratively shrinking the set, by means of searching for an integer vector a_{s+1} in $\Omega_2(\chi_s^2)$ that provides a smaller value for $\chi_{s+1}^2 = C_2(a_{s+1}) < C_2(a_s) = \chi_s^2$, until the minimizer of $C_2(a)$ is found. The minimizer of $C(a)$, which may differ from the one of $C_2(a)$, is then extensively searched inside the shrunken set

$$\Omega(\tilde{\chi}^2) = \left\{ a \in \mathbb{Z}^n | C(a) \le \tilde{\chi}^2 \right\} \supseteq \Omega_2(\tilde{\chi}^2) \tag{18}$$

where $\tilde{\chi}^2 = C_2(\tilde{a})$, being $\tilde{a}$ the minimizer of $C_2(a)$.

The two search strategies provide an efficient way of performing the search for the integer minimizer of (13), by overtaking both the issues of fixing the initial size of the search space, and speeding up the search avoiding the computation of the constrained least squares minimizer a large number of times. Both methods are less sensitive to the choice of the initial value of χ than the exhaustive search: the size of the search space is iteratively adjusted by expanding or shrinking, working on functions that do not require the evaluation of a constrained least squares problem. The two methods aim to have a final small set $\Omega(\chi^2)$ where the integer minimizer of (13) is quickly extracted.

The sharpness of the selected bounds is an important aspect, since tighter bounds effectively reduce the time dedicated to the computation of (13), thus resulting in a faster global search for the integer minimizer. Both techniques are proved to work efficiently, with a computational load comparable to the one of the LAMBDA method.

The advantage of the C-LAMBDA method lies in the major strength of the functional model. The baseline coordinates are constrained by the knowledge of the distance between the antennas. Embedding this information in the ambiguity resolution process enormously benefits the search for the correct integer ambiguity vector. This allows to downgrade the GNSS equipment requirement in case of configurations of antennas firmly installed on a ship.

We used the baseline constraint above as a "hard" constraint. If the need arises though, one can loosen the constraint and obtain a weighted constrained ILS approach, as is shown in [14].

C. A Linearized Version of the Constrained Solution

For long baselines applications, e.g., big oil tankers or container ships, a linearized version of (13) is worthy of consideration. The linearized expression is derived from a Taylor expansion of the objective function, based on the constrained ambiguity solution $\bar{a}$ [14]. The constrained float estimates $\bar{a}$ and $\bar{b}$ are obtained from the unconstrained float solution according to [14]

$$\begin{aligned} \bar{b} &= \arg \min_{b \in \mathbb{R}^3, \|b\|=l} \|\hat{b}-b\|^2_{Q_{\hat{b}\hat{b}}} \\ \bar{a} &= \left(A^T Q_{yy}^{-1} A\right)^{-1} A^T Q_{yy}^{-1}(y - B\bar{b}). \end{aligned} \tag{19}$$

The linearized approximation of the cost function reads

$$\begin{aligned} C(a) &= \|\hat{a}-a\|^2_{Q_{\hat{a}\hat{a}}} + \left\| \hat{b}(a) - \check{b}(a) \right\|^2_{Q_{\hat{b}(a)\hat{b}(a)}} \\ &\approx C(\bar{a}) + (\bar{a}-a)^T \left(\frac{1}{2} \partial^2_{aa} C(\bar{a}) \right) (\bar{a}-a) \end{aligned} \tag{20}$$

where $\partial^2_{aa} C(\bar{a})$ is the Hessian of the objective function (13) evaluated at $\bar{a}$. The performance of (20) depends upon the baseline length. The geometrical interpretation of (13) gives an explanation to the latter statement: the nonlinearity of the constrained method is due to the curved manifold upon which the baseline solution is projected. This manifold is the sphere of radius equal to the baseline length l. Thus, longer baselines yield to smaller curvature and lower local nonlinearity. Following (20), the minimization problem is reformulated as

$$\check{a} = \arg \min_{a \in \mathbb{Z}^n} \|\bar{a}-a\|^2_{\left(\frac{1}{2}\partial^2_{aa} C(\bar{a})\right)^{-1}}. \tag{21}$$

Expression (21) is a quadratic integer minimization problem, and the standard LAMBDA method applies. For its simplicity,

the linearized method is of interest for those applications where the baseline is longer than a certain threshold. This is investigated during the experimental verification of the method.

D. Attitude and UKC Estimations

The precise baseline estimation, obtained by resolving the carrier-phase ambiguities, enables to derive both the attitude of the ship and its relative position with respect to a reference point (RTK). The GNSS receivers placed aboard the ship also provide absolute vertical motions relative to a fixed vertical reference on Earth, to be used in combination with nautical chart datum to estimate the UKC.

1) Attitude Determination: The attitude of a body is represented by defining a rotation matrix that linearly relates the baseline coordinates expressed into different (orthogonal) frames. For the applications of this study, the frames considered are the east-north-up (ENU) frame enu and the local frame uvw. The latter is so characterized: the first axis is aligned with the longitudinal direction on the boat, the second axis is perpendicular to the first, lying in the local horizontal plane, and the third axis is directed so to form a right-handed orthogonal frame. The attitude matrix may be expressed with different parameterizations, such as the direct cosine matrix (DCM), the Euler angles, the quaternions, or the Gibbs vector [28]. In this contribution, the Euler angles parameterization is used, which has a direct physical interpretation. The rotation matrix is built performing three ordered right-handed rotations, each one made about one of the main axis, to coalesce the frame enu with the local frame uvw. The sequence 321 is used: the first rotation (heading, ψ) is about the third axis w, the second (pitch, θ) is about the second axis v, and the last (roll, ϕ) is about the first axis u. The relationship between the coordinates of the baseline i before (b) and after (b_b) the transformation is

$$b^i = R \cdot b^i_b, \qquad \text{with } R(\psi,\theta,\phi) = R_3(\psi)R_2(\theta)R_1(\phi). \quad (22)$$

Given k observed baselines, the estimation of the rotation matrix can be addressed as the solution of the LS problem

$$\check{R} = \arg \min_{R \in \mathbb{O}^{3\times 3}} \sum_{i=1}^{k} \left\| b^i - R \cdot b^i_b \right\|, \qquad \text{with } \det(\check{R}) = +1 \quad (23)$$

where $\mathbb{O}^{3\times 3}$ denotes the class of the 3×3 orthogonal matrices. Expression (23) is known in literature as the *Wahba's problem* [29]. A closed-from solution of this problem is known and it is reviewed in the Appendix.

2) UKC Estimation: The measured vertical position and attitude of a ship can be directly used in ship UKC monitoring, when combined with the known local bathymetry. Ship UKC is influenced by many factors, including squat (the bodily sinkage and change in trim of a ship with increasing forward speed), wave-induced heave, pitch and roll, as well as heel due to wind or turning. A diagrammatic representation of the components of ship UKC is shown in Fig. 2. The factors affecting ship UKC are discussed in [30]. For ships in shallow areas where the seabed is locally horizontal, grounding risk is determined by the water depth beneath chart datum and the point on the ship's keel having the lowest vertical elevation at a given instant. For large

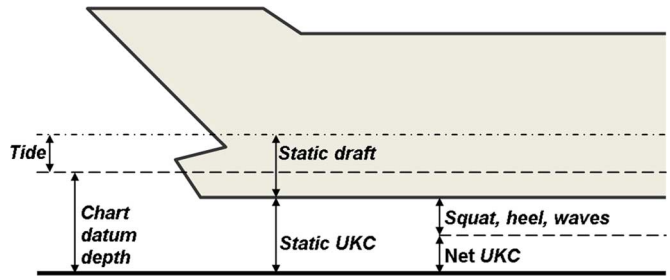

Fig. 2. Schematic illustration of the components of ship UKC.

cargo ships, the baseline (keel) of the ship is flat over a large area, such that any point around the perimeter of the keel can be at risk of grounding, depending on the initial trim and the relative phasing between heave, pitch, and roll of the ship.

In areas where the seabed is locally flat but not horizontal, the points around the perimeter of the keel are still most at risk of grounding, though the varying water depth around this perimeter must be considered. For an irregular seabed (e.g., consisting of rock pinnacles), grounding may occur at any point on the keel as the ship heaves, pitches, and rolls with forward speed. A comprehensive UKC analysis should therefore consider the vertical elevation of the entire keel planform, however UKC calculations have previously been simplified to just considering the ship's bow [31].

Some recent ship groundings in shallow water demonstrate the need for a whole-ship approach to UKC. These include the groundings of *Eastern Honor* [32], which occurred mainly at the stern of the ship, *Capella Voyager* [33], which occurred at the bow, and *Jody F Millennium* [34], which occurred at each of the bilge corners (transverse extremities of the keel). All of these ships had a positive "static UKC" (see Fig. 2), but squat and wave-induced heave, pitch, and roll caused parts of the hull to touch bottom and sustain significant damage.

As described in Section II-D1, the RTK GPS positions of the shipboard receivers, together with their positions in the local ship reference frame, are the inputs for attitude determination. These are then transformed into the instantaneous heading, pitch, and roll of the ship, together with the position in ENU coordinates of a predetermined location on the ship (e.g., the center of gravity). This process can now be reversed to find the position in ENU coordinates of a matrix of locations on the ship's keel, starting with their position in the local ship reference frame and using the instantaneous ship heading, pitch, roll, and center of gravity position in ENU coordinates. The ENU coordinates of a matrix of positions on the ship's keel can then be compared with the charted bathymetry of the area (also in ENU coordinates) to determine the instantaneous distance between each point on the keel and the seabed directly beneath it.

The application of GNSS-based methods to ship UKC monitoring is likely to become of increasing importance over the following decade. The economies of scale with respect to ship sizes, versus the cost of dredging, are leading to tighter tolerances on allowable static UKC. The methods used to determine allowable UKC are only approximate, so much further validation and refinement of these methods is required, for which

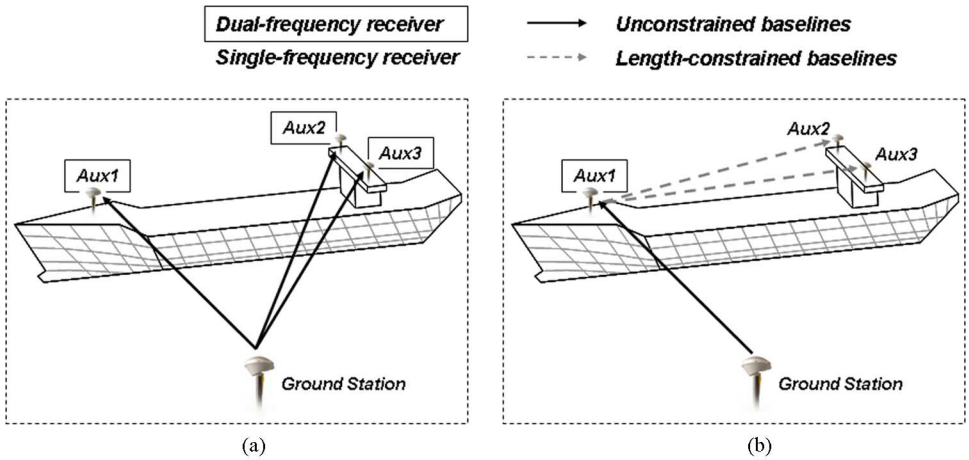

Fig. 3. Scheme of a (a) classical RTK approach with four dual-frequency antennas/receivers compared to the (b) low(er)-cost solution, where the number of dual-frequency equipment is halved.

GNSS is the ideal measurement tool. Real-time GNSS measurements may also be used to help predict UKC a short time into the future, providing a warning to the ship if UKC values fall below those predicted in the passage planning.

Currently, most shipping channel bathymetry is provided at a fairly coarse spatial resolution, such that depth changes over the length of a ship cannot be accurately quantified. Therefore, a conservative approach in the interim is to use the "least depth" over the ship's footprint, combined with the lowest vertical elevation of the keel perimeter, in determining UKC. As charted bathymetry improves in spatial resolution (limited in many areas by the constant depth changes due to siltation), the ENU coordinates of the seabed and instantaneous keel platform locations can be used for determining instantaneous UKC values over the entire hull.

3) Dual- Versus Single-Frequency GNSS Receivers Configurations: The strengthening of the underlying GNSS observation model via the inclusion of the nonlinear geometrical constraint allows to downgrade the equipment aboard the ship for attitude determination and UKC estimation: only one dual-frequency receiver is needed to reliably obtain an RTK solution, and another two (or more) single-frequency receivers are employed to compute the attitude. Fig. 3 clarifies the distinction between a classical RTK approach and the new method, which exploits the known baseline separations. The second configuration allows to halve the number of (expensive) dual-frequency GNSS receivers aboard, maintaining the same reliability and accuracy of the most expensive configurations.

III. Experimental Testing

The methods presented were tested during different experiments, carried out at different locations, time, and external conditions. Different types of GNSS receivers were employed. A static test in Perth, W.A., Australia, provided indication over the performance achievable varying the baseline length and the number of satellites in view. A kinematic test was performed in The Netherlands, where a small boat was sailed along the Schie Canal, Delft. The final test was performed in the harbor of Hong Kong, where antennas installed aboard few large container ships provided the precise position and attitude during the inbound and outbound maneuvers.

Different performance indicators were extracted. First, it was investigated the unaided single-epoch, single-frequency success rate, i.e., the capacity of fixing the correct set of ambiguities when processing single-epoch data, collected on GPS-L1 frequency, without any external aid (e.g., inertial sensors, gyros, etc.) or filtering. High values for this parameter mean higher robustness and shorter times to fix. Quick recoveries of the correct ambiguities after a cycle slip or loss of lock are of primary importance for those applications that rely on real-time GNSS precise position estimates.

Based on the resolved ambiguities, the precise baseline vectors were used to derive the ships' position and attitude. The accuracy of the baseline solution was tested through a static test. In the Hong Kong test, the solution was compared to the output of a commercial software (TGO, Trimble Geomatic Office, Sunnyvale, CA) for benchmarking.

Finally, the timing performance of the ambiguity resolution methods is reported, to stress the efficiency of the algorithms presented.

A. Static Data Set

The static test was performed at the Curtin University of Technology (CUT, Perth, W.A., Australia) campus. Several baselines were formed by lining up antennas from a known reference point. The antennas/receivers (Sokkia GSR 2700 ISX) were placed at regular intervals from 0.6 to 100 m (Fig. 4). Six receivers were used for the test, and four different measurement sessions were planned. Five different baselines were tested at each session, allowing two overlaps between consecutive sessions. The ground truth for the experiment was surveyed with a Sokkia Set1X total station (2-mm distance measurement accuracy). The number of satellites tracked varied between six and nine (Fig. 5), with position dilution of precision (PDOP) values ranging between 2.2 and 3 most of the time, with a peak of 16 during the first 800 epochs of the first session, due to a bad distribution of the six tracked satellites in the sky. The

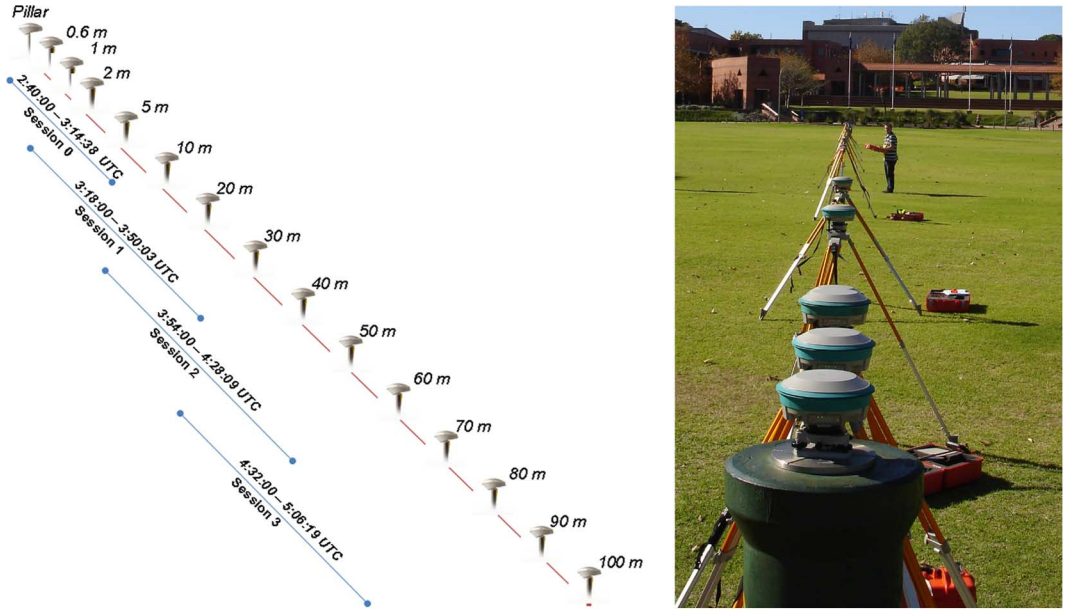

Fig. 4. The static test performed at the CUT campus, lining up 15 receivers at distances between 0.6 and 100 m from a reference point (pillar). (a) Scheme of the receivers placement for each session. (b) Picture of the 15 lined-up tripods.

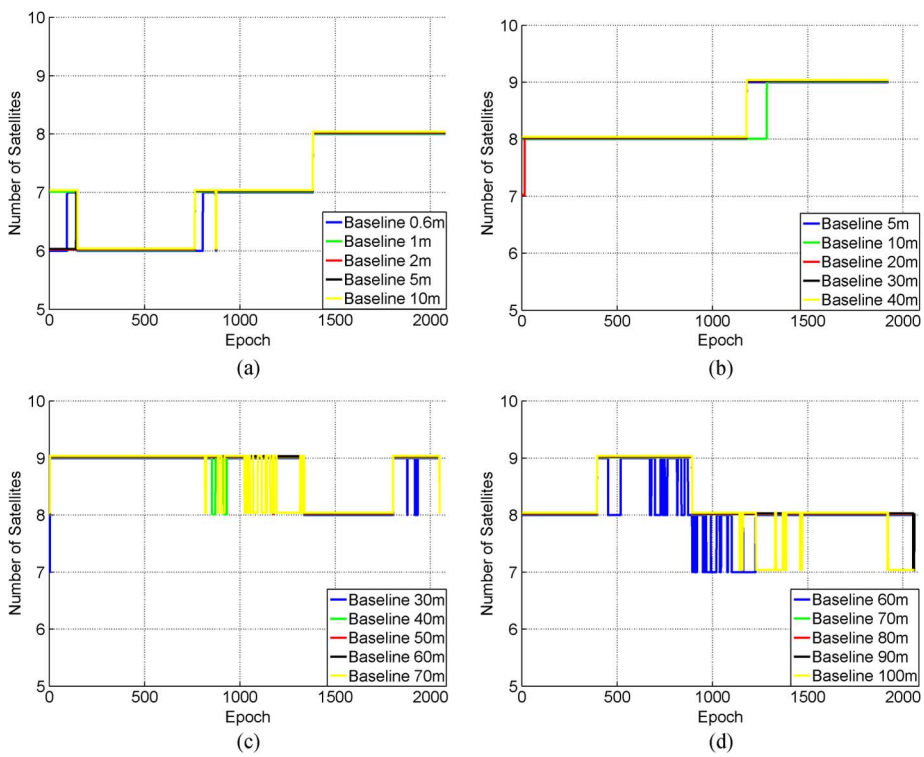

Fig. 5. Static test: number of tracked satellites at each baseline/session. (a) Session 0. (b) Session 1. (c) Session 2. (d) Session 3.

data sets collected were processed with the LAMBDA and C-LAMBDA methods. Results obtained applying the linearized version (LC-LAMBDA, discussed in Section II-C) are given, investigating how the baseline separation between the antennas affects its performance.

1) Success Rate Performance: First, we looked into the unaided, single-frequency, single-epoch success rate, i.e., the ratio of correctly fixed integer vectors in the tested time span. The data were processed epoch by epoch, thus not using any filtering or batch computation. Also, only GPS L1 data were used. Table I compares the results obtained with the three methods. The first session was characterized by a lower average number of satellites (see Fig. 5), which explains the lower success rate of the LAMBDA method. The constrained method was capable of fixing the correct ambiguities for 99% of the time for most of the data sets. The C-LAMBDA method showed a larger ro-

TABLE I
STATIC DATA SET: UNAIDED SINGLE-FREQUENCY, SINGLE-EPOCH SUCCESS RATES FOR THE LAMBDA, C-LAMBDA, AND LC-LAMBDA METHODS, AS A FUNCTION OF THE SESSION/BASELINE LENGTH

	Epochs	Baseline length [m]	Unaided single-frequency, single-epoch success rate [%]		
			LAMBDA	C-LAMBDA	LC-LAMBDA
Session 0	2079	0.598	76.5	98.6	13.2
		1.000	76.8	99.7	10.7
		1.999	74.2	97.7	12.9
		4.999	75.5	99.1	27.5
		10.001	77.8	99.0	34.8
Session 1	1924	4.999	90.6	99.9	28.7
		10.001	90.5	99.6	41.4
		20.004	96.6	99.8	58.2
		30.008	98.1	99.9	71.4
		40.010	98.6	99.9	82.6
Session 2	2050	30.008	86.2	99.5	69.6
		40.010	93.6	99.9	81.1
		50.010	78.0	99.7	84.0
		60.017	89.0	99.9	87.2
		70.018	90.1	96.1	85.5
Session 3	2060	60.017	64.7	98.9	82.7
		70.018	85.6	99.8	91.5
		80.020	87.4	99.9	94.2
		90.024	75.9	99.1	90.6
		100.032	61.6	99.8	84.6

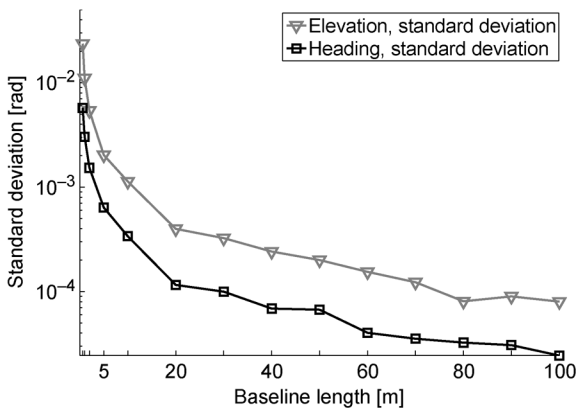

Fig. 6. Standard deviations of the heading and elevation angles as a function of the baseline length, static test.

bustness against the satellite configuration, due to the increased strength of the underlying model.

As expected, the linearized method provided acceptable results only for baselines longer than a certain threshold. This threshold, according to the static test, is located between 40 and 60 m. It is noteworthy that for longer baselines the linearized method provided higher success rates than the standard approach. This was as expected, since the nonlinearity of the stronger constrained model largely reduces on longer baselines.

2) Accuracy Performance: The set of (correctly) fixed ambiguities gives very precise baseline coordinates estimation, according to (8). However, the precision of the attitude angles also depends on the baseline separation between the antennas. Fig. 6 shows the standard deviations of the heading and elevation angles for the static data sets as a function of the baseline length. As expected, both angles were estimated with higher accuracy at longer baseline lengths. For the shortest baseline examined, 0.6 m, the standard deviation of the estimated attitude angles did not exceed one degree. The elevation angle was estimated with higher uncertainty due to the properties of the GNSS working principle: the satellites cover, with respect to the receiver, only a hemisphere, causing higher dilution of error in the vertical plane.

3) Timing Performance: Deriving a solution in a timely manner is fundamental for real-time applications. The time to resolve the vector of ambiguities was extrapolated from the implemented software. Although the code is not optimized, the timing performance shows the quickness of the new method: on average, each epoch of data was resolved[1] within 2.44 ms with the LAMBDA method, 3.57 ms with the C-LAMBDA method, and 2.55 ms with the LC-LAMBDA method. The constrained method, which was expected to be slower due to the higher complexity of the search algorithm, does not show a significant displacement from the timing performance of the linear methods. This is achieved thanks to the sharp bounds and efficient search strategies, described in Section II-B.

B. Testing on a Small Boat Sailing a Canal

A precise absolute positioning system is important for small vessels where the exact track, speed, and attitude need to be recorded, e.g., for maneuvering trials, speed trials, boat wake trials, or automatic navigation. The GNSS RTK solution provides centimeter-level accuracy in the estimation of the boat position. This section presents the results obtained by applying the methods described earlier to an experiment performed with a small boat sailing the narrow Schie Canal.

The boat in Fig. 7(a) was equipped with three antenna/receiver couples: a choke-ring antenna connected to an Ashtech

[1]Data processed in Matlab, v.7.5, running on a Pentium Core2, 2.15-GHz, 2-Gb RAM.

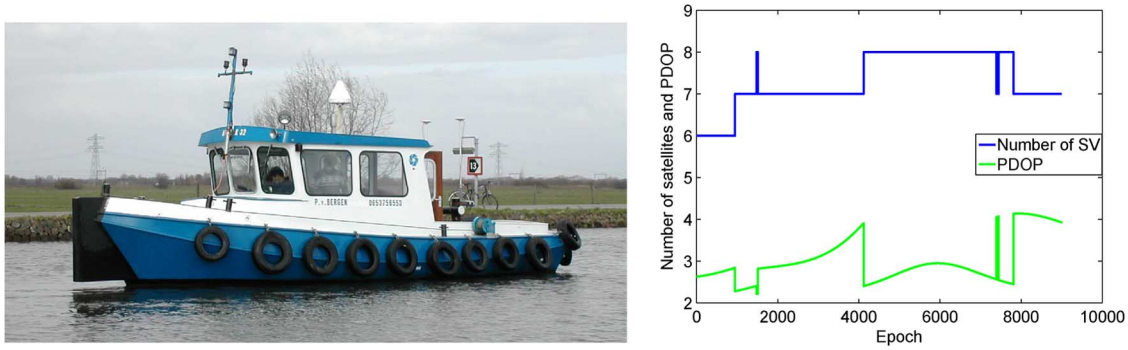

Fig. 7. The Schie experiment: three antennas/receivers were carried aboard a small boat sailing the Schie Canal, Delft, The Netherlands. (a) The boat used for the Schie experiment, equipped with three antenna/receiver couples. (b) The number of tracked satellites and PDOP values.

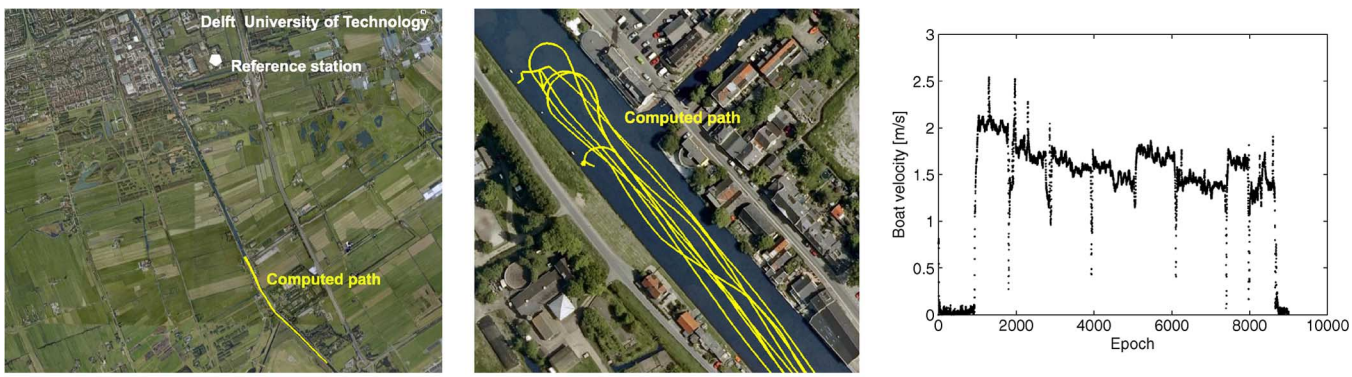

Fig. 8. Schie experiment: the path followed by the boat is precisely computed by resolving the ambiguities between a reference station and one of the antennas aboard. The speed of the boat is accurately derived by differencing the position estimates. (a) Image of the experiment setup, showing the DUT campus, the reference station, and the path of the boat. (b) Part of the boat's sailing path. (c) The boat absolute velocity profile.

TABLE II
SCHIE DATA SET: UNAIDED SINGLE-FREQUENCY, SINGLE-EPOCH SUCCESS RATES FOR THE LAMBDA AND C-LAMBDA METHODS

	Baselines	*LAMBDA*	*C-LAMBDA*
Single-epoch , single frequency, single baseline success rate [%]	1-2	82.0	99.6
	1-3	61.7	97.7

receiver, an antenna connected to a Leica SR530 receiver, and a third antenna connected to a Novatel OEM3 receiver. The baseline lengths between the antennas were 2 m (Ashtech-Leica) and 1.5 m (Ashtech-Novatel). The boat was sailed for about 2.5 h, collecting 9000 epochs of GPS-L1/L2 code and phase observations. The number of tracked GPS satellites varied between 7 and 8, except for the first 1000 epochs, where data from only six satellites were stored. The PDOP values varied between 2.1 and 4.1 [Fig. 7(b)].

1) Success Rate Performance: Table II summarizes the unaided single-frequency, single-epoch success rate obtained by processing the data sets with the LAMBDA and C-LAMBDA methods (the linearized method should not be applied, since the baseline lengths are too short). The improvement obtained by exploiting the additional nonlinear geometrical constraint is evident: the number of correctly fixed epochs increased from 82% to 99.6% for the first baseline and from 61.7% to 97.7% for the second baseline. It is evident that dual-frequency equipment is not necessary when the model can be made sufficiently strong by rigorously including additional constraints that drive the ambiguity resolution process.

Dual-frequency data are useful, however, to derive the RTK solution, where no constraints can be exploited and the single-frequency model lacks sufficient strength. For this experiment, a reference station was available within 6 km from the boat sailing path, and a precise relative position could be computed at each epoch applying the dual-frequency (unconstrained) model (10). All the ambiguities were correctly fixed, and Fig. 8(a) and (b) shows the path of the boat on a map. The RTK solution also provides an estimate of the boat speed, whose time series is plotted in Fig. 8(c).

2) Attitude Estimation: Fig. 9 illustrates the three attitude angles (heading, pitch, and roll) derived with the two fixed baseline vectors aboard. Since the correct attitude estimation is obtained only when both baselines are correctly fixed, the ratio of epochs where the single-epoch attitude solution was available equals 97.4%. It is remarkable that using the C-LAMBDA method to process L_1-only observations provided such high

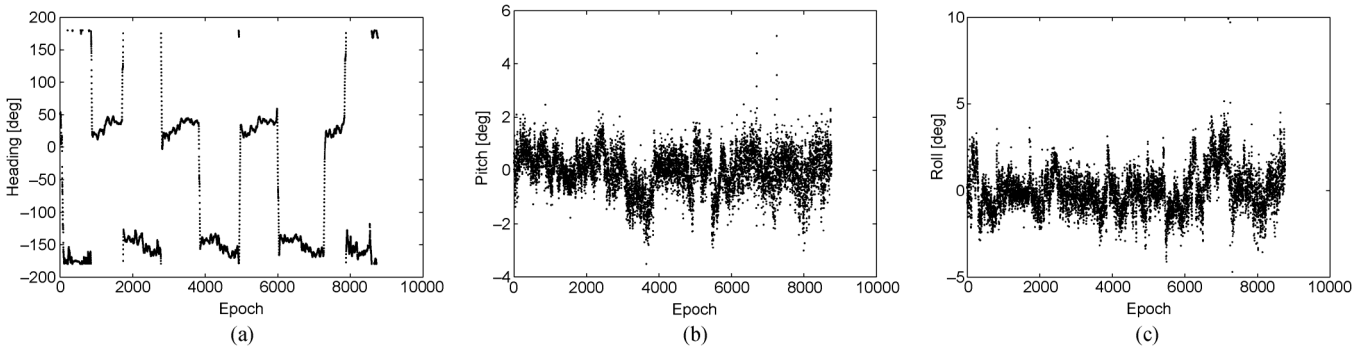

Fig. 9. Schie experiment: the GNSS-based full attitude solution. (a) Heading angle. (b) Pitch angle. (c) Roll angle.

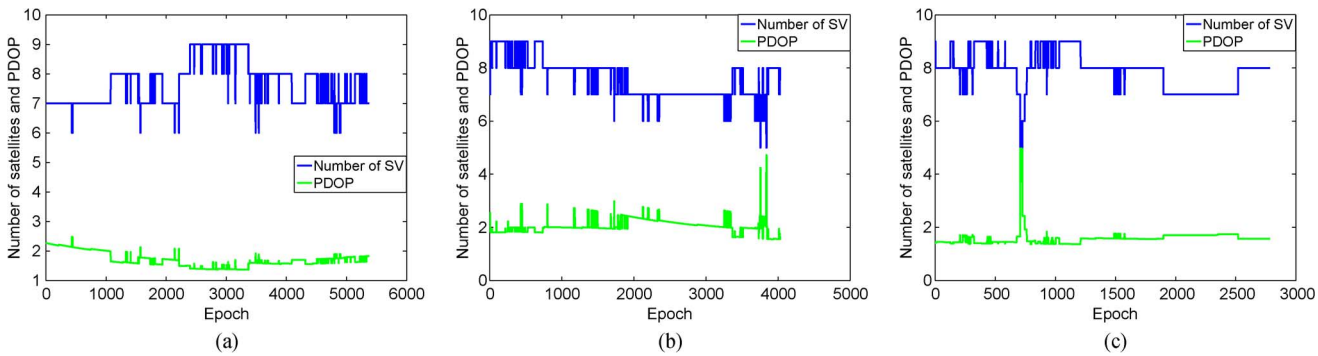

Fig. 10. Hong Kong test: number of tracked satellites and PDOP values for each ship. (a) *Katrine Maersk*. (b) *Maersk Dortmund*. (c) *Sally Maersk*.

TABLE III
HONG KONG DATA SETS: GENERAL INFORMATION ABOUT THE SHIPS INVOLVED IN THE EXPERIMENT

Ship	Length [m]	Transit direction	Displacement [tonnes]	Test date and time (GMT)
Katrine Maersk	318	Inbound	107200	12/02/2005 00:48 - 02:18
Maersk Dortmund	294	Inbound	55000	05/02/2005 00:39 - 01:46
Sally Maersk	347	Outbound	111300	08/02/2005 01:41 - 02:27

success rate on a single-epoch base, without any external aid or any filtering of the data. This allows on-the-fly attitude estimations and real-time control with high reliability, since the algorithm can quickly recover from any fault.

3) Timing Results: The fast convergence of the constrained algorithm was confirmed also in this kinematic experiment: LAMBDA took on average 2.2 ms to extract the integer minimizer in both baselines, while the C-LAMBDA method employed on average 5.0 ms (first baseline) and 5.5 ms (second baseline), a small increment due to the higher complexity of the algorithm.

C. Testing on Large Container Ships Approaching the Hong Kong Harbor

In 2005, the Centre for Marine Science and Technology, CUT, performed a series of tests for the Hong Kong Marine Department. A detailed study of the sinkage and dynamic draft of container ships entering and leaving Kwai Chung, the busiest container port in the world, was performed. Full-scale trials were carried out on some of the largest container ships, ranging in overall length from 294 to 352 m, to accurately measure sinkage, trim, and roll [4], [5]. Three receivers/antennas (Trimble 5700 receivers connected to Trimble Zephyr antennas) were installed aboard the ships, one at the bow, two on the bridge (one at port and one at starboard side). A ground station was setup at the berth (of the same manufacturer and type of the antennas aboard). Table III reports some information about three example ships involved in the experiment, while Fig. 10 shows the number of (common) tracked satellites from the antennas and PDOP values.

For each ship, the precise absolute position as well as its attitude (heading, roll, and pitch) was computed. In the following, various aspects of the proposed method are analyzed, and a comparison with the results obtainable with a commercial software is provided.

TABLE IV
HONG KONG DATA SETS: UNAIDED SINGLE-FREQUENCY, SINGLE-EPOCH SUCCESS RATES FOR THE LAMBDA, C-LAMBDA, AND LC-LAMBDA METHODS

Ship	Baseline	length [m]	Unaided single-epoch, single frequency, single baseline success rate [%]		
			LAMBDA	C-LAMBDA	LC-LAMBDA
Katrine Maersk	Port to Bow	213.91	16.4	76.4	74.7
	Starboard to Bow	213.86	16.8	75.7	72.7
	Port to Starboard	42.515	38.5	93.4	67.8
Maersk Dortmund	Port to Bow	223.51	14.1	61.5	60.6
	Starboard to Bow	223.53	17.6	75.6	65.1
	Port to Starboard	30.270	12.1	69.8	27.9
Sally Maersk	Port to Bow	242.23	19.9	80.5	79.4
	Starboard to Bow	242.22	16.9	71.6	66.5
	Port to Starboard	36.090	32.6	89.5	58.6

(a) (b) (c)

Fig. 11. Picture of the antennas aboard one of the Maersk ships. (a) The antenna installed at the bow. (b) The antenna installed above the bridge, starboard side. (c) The antenna installed above the bridge, port side.

1) Success Rate Performance: The feasibility of real-time monitoring of ship sinkage and attitude is dependent on the single-epoch performance of the ambiguity resolution method, which has to guarantee a quick correct solution. Table IV reports the single-frequency, single-epoch success rates for each of the baselines between antennas carried aboard. All the baselines formed by the three antennas on the ship were processed with the LAMBDA, C-LAMBDA, and LC-LAMBDA methods. The improvement in success rate from the LAMBDA method to the C-LAMBDA or LC-LAMBDA methods was rather large for all the cases, showing that the inclusion of the baseline length as a constraint in the ambiguity resolution process leads to a large improvement in the capacity of resolving the correct set of carrier-phase ambiguities. The single-epoch results for all the methods showed reduced performance with respect to the previous Schie test, the reason being the quite different surrounding environment. The pseudorange and carrier-phase measurements were more affected from multipath, being surrounded by the metal structure of the vessel and the containers (Fig. 11). Noteworthy, the constrained method was capable of largely improving the success rate also in such environment.

The linearized method, due to the long baselines of the test, always provided higher success rate than the standard LAMBDA method, and approaching the performance of the C-LAMBDA method for the longest baselines. This makes the LC-LAMBDA method rather interesting for this class of vessels, where baselines usually are tens or hundreds of meters long.

Although our method of constraining has significantly improved the ambiguity success rate performance, for reliable ambiguity resolution of course higher success rates are needed than shown in Table IV. Note though that these are unaided, single-epoch success rate values. Hence, in case of multiepoch processing, our success rates will achieve acceptable levels in only a few epochs.

2) Attitude Estimation and Relative Positioning: The correct set of integer ambiguities provides precise baseline coordinates vector. The ship full attitude is then extracted from the vector observations. Fig. 12 shows the three attitude angles for each ship: heading (with respect to the north direction), roll, and pitch. The angles were derived from single-epoch baseline observations resolved with the C-LAMBDA method, using the approach described in Section II-D1.

To compare the quality of the obtained estimation, a comparison with a commercial software (Trimble Geomatic Office, TGO) is provided. Fig. 13 shows the differences between the attitude angles obtained with the C-LAMBDA method and derived making use of the baseline solutions resolved by the TGO software. The performance of the C-LAMBDA method matches the one of the TGO software, with small deviations

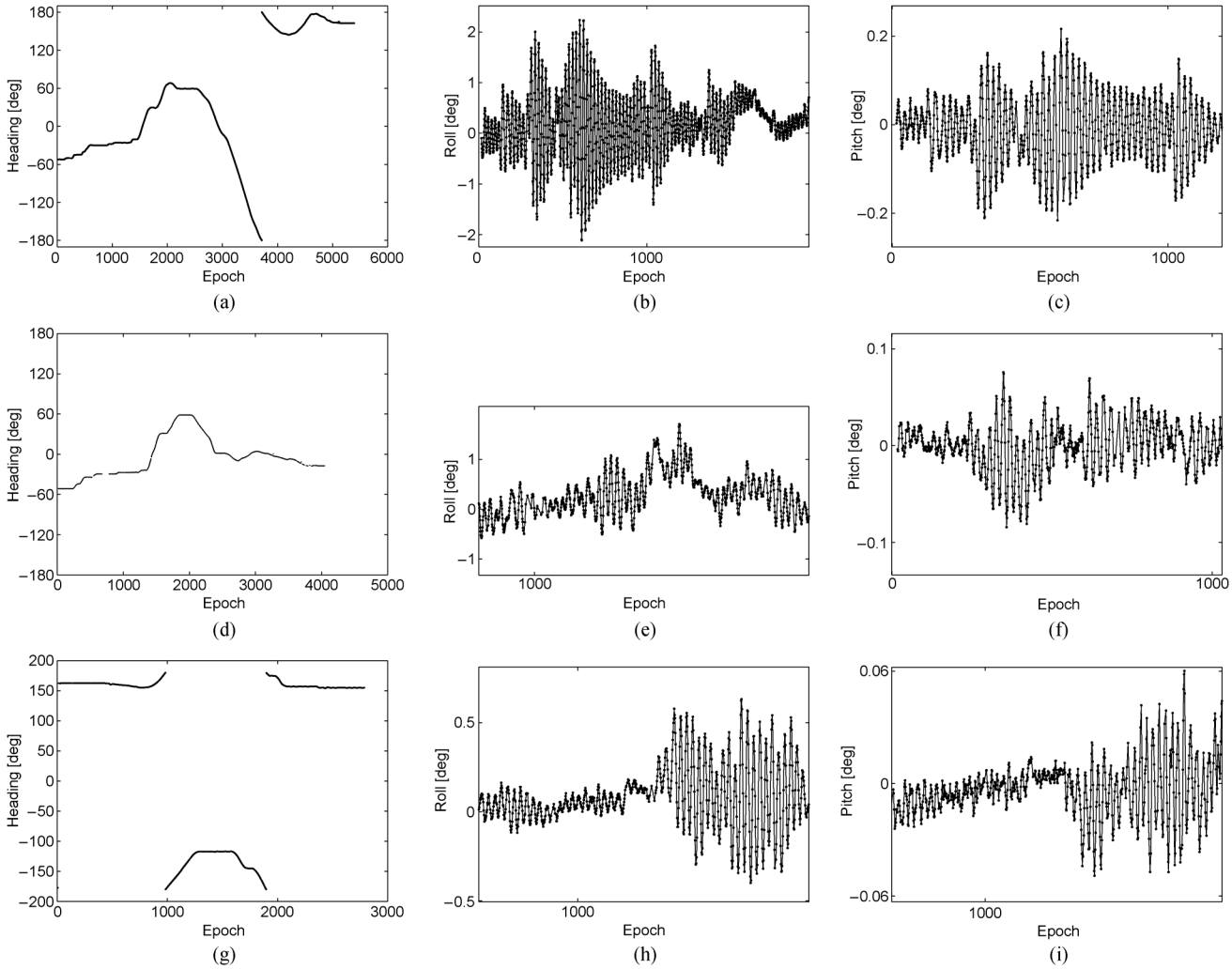

Fig. 12. The three attitude angles computed with the C-LAMBDA method for each ship examined. Only a part of the roll and pitch time series has been reported, to better visualize the oscillating behavior. (a) Heading angle, *Katrine Maersk*. (b) Roll angle, *Katrine Maersk*. (c) Pitch angle, *Katrine Maersk*. (d) Heading angle, *Maersk Dortmund*. (e) Roll angle, *Maersk Dortmund*. (f) Pitch angle, *Maersk Dortmund*. (g) Heading angle, *Sally Maersk*. (h) Roll angle, *Sally Maersk*. (i) Pitch angle, *Sally Maersk*.

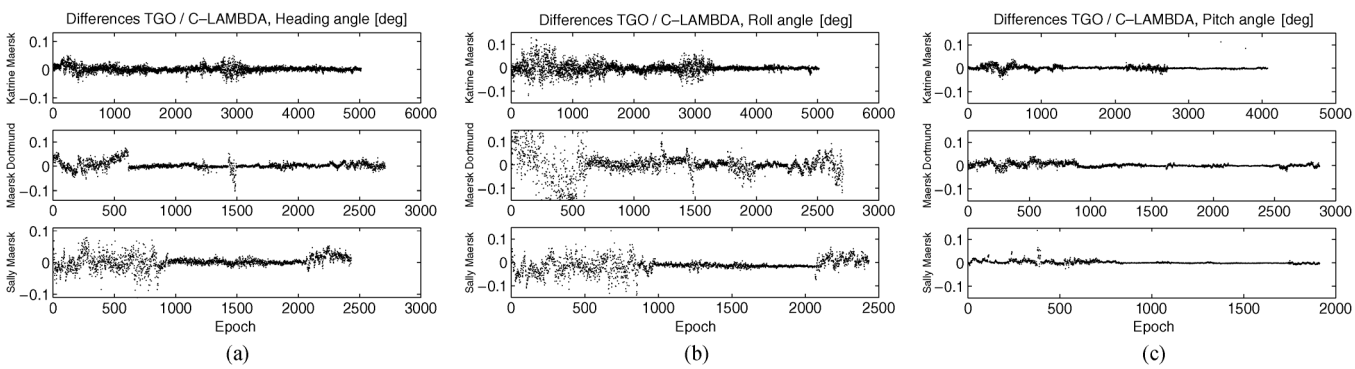

Fig. 13. Comparison between the attitude results obtained with the C-LAMBDA method and with the TGO software. The differences are contained within 0.15° in all the cases. (a) Heading angle, differences between C-LAMBDA and TGO. (b) Roll angle, differences between C-LAMBDA and TGO. (c) Pitch angle, differences between C-LAMBDA and TGO.

between the different estimations: the differences are mostly contained within 0.05°, and never exceed 0.15°. This suggests that the proposed algorithm can perfectly compensate a downgrade of the equipment carried aboard: the results obtained processing single-epoch, single-frequency observations and without applying any filtering or dynamic modeling match those obtained with a commercial software that processes dual-frequency observations on a multiepoch base.

However, a dual-frequency receiver is necessary aboard to obtain a reliable and precise (centimeter-level) RTK solution

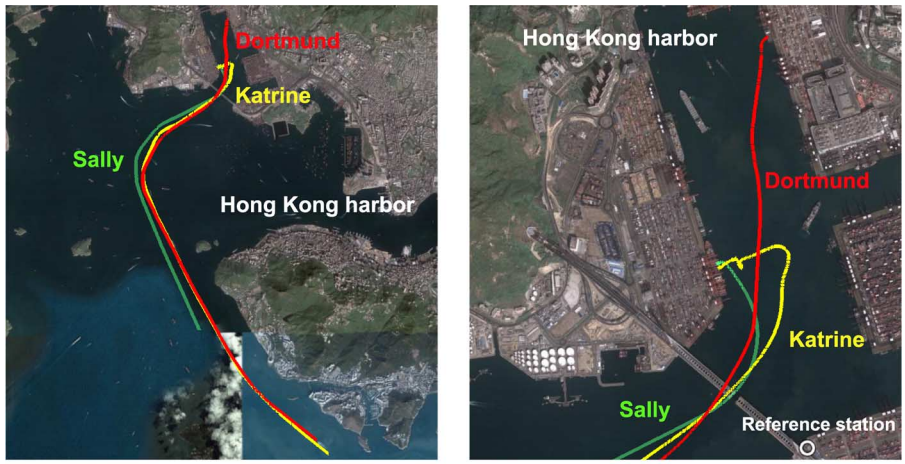

(a) (b)

Fig. 14. Hong Kong test: the trajectory of the three ships approaching (*Katrine* and *Dortmund*) or leaving (*Sally*) the quay, Hong Kong harbor. (a) The trajectory of the three ships during the experiment. (b) The three ships entering or leaving the anchorage area. The ground station is visualized as well.

TABLE V
HONG KONG DATA SETS: AVERAGE SINGLE-EPOCH COMPUTATION TIME FOR THE LAMBDA, C-LAMBDA, AND LC-LAMBDA METHODS

Ship	Baseline	Average single-epoch computational time [ms]		
		LAMBDA	C-LAMBDA	LC-LAMBDA
Katrine Maersk	Port to Bow	2.5	6.1	2.4
	Starboard to Bow	2.4	6.0	2.4
	Port to Starboard	2.5	4.5	2.5
Maersk Dortmund	Port to Bow	2.3	6.9	2.2
	Starboard to Bow	2.4	6.0	2.4
	Port to Starboard	2.3	6.3	2.2
Sally Maersk	Port to Bow	2.6	6.2	2.5
	Starboard to Bow	2.6	6.5	2.4
	Port to Starboard	2.5	4.9	2.5

for the ships. Fig. 14 shows the trajectories of the three ships entering (*Katrine* and *Dortmund*) or leaving (*Sally*) the quay, at the Hong Kong harbor. This precise RTK solution can be coupled to the attitude estimations to provide real-time UKC monitoring if precise depth data are available.

3) Timing Performance: Table V reports the time elapsed during the ambiguity search for the various methods tested. The C-LAMBDA method, due to its inherent complexity, required only slightly longer searches. The linearized method marked timing results even faster than the one of the original LAMBDA method, thanks to the simplified cost function associated to the stronger—for long baselines—underlying model.

IV. CONCLUSION

This contribution reports field-test results of a newly developed method for GNSS carrier-phase ambiguity resolution. The process of resolving the ambiguities inherent to the GNSS carrier-phase observables is the key toward very precise (up to millimeter-level) positioning products. The LAMBDA method is an optimal algorithm to resolve the integer ambiguities, and widely used for its computational efficiency. For those applications where the baselines between the antennas are precisely known, it is desirable to exploit the *a priori* information to drive the ambiguity resolution process, rather than using it only for validation purposes or to obtain a more accurate float solution. The C-LAMBDA method, an extension of the LAMBDA method for baseline-constrained models, has been introduced with the objective of rigorously resolving the unknown ambiguities for frames of antennas firmly mounted aboard moving platforms. The *a priori* information is embedded into the ambiguity resolution process, via a modification of the cost function to be minimized by the search algorithm. The strengthening of the observation model reflects into an improved capacity of fixing the correct set of integer ambiguities, if compared to the classical unconstrained algorithms. This allows the user to match the performance usually obtainable only with dual-frequency equipment by using only single-frequency receivers/antennas and still providing a reliable baseline solution on an epoch-by-epoch base.

The application subject of this paper is the estimation of ship attitude and UKC. To estimate the distance between a ship's hull and the seabed, the absolute position of one point on the ship has to be first precisely determined, to locate the ship on a nautical chart datum. Then, the attitude of the ship is estimated to detect the deepest point of the hull and avoid collisions with any of the seabed features.

The method presented in this work makes use of only two dual-frequency receivers (one onboard, one onshore) to precisely estimate the ship's position. Then, a set of two or more single-frequency receivers/antennas onboard is required to estimate the hull's attitude. The use of lower grade equipment is compensated by the higher strength of the functional model if the set of geometrical constraints posed on the baselines is embedded into the ambiguity resolution algorithm.

Various test results showed that the C-LAMBDA method matches the performance obtainable with classical RTK multi-frequency configurations, allowing a fast, reliable, and precise estimation of the ship's attitude with reduced costs.

A linearized version of the method is also tested: the LC-LAMBDA method is demonstrated to be a valid procedure to perform ambiguity resolution for long baselines. It avoids the complex search associated to the constrained method, although exploiting the stronger functional model by means of extracting the constrained float solution and a modified cost function. Both experimental success rates and timing performance suggest that the method should be employed to all those RTK applications making use of known long (tens or hundreds of meters) baselines; such is the case with attitude determination of large vessels.

Numerous maritime applications could benefit from the methods described in this work, ranging from the automatic port navigation to precise docking assistance.

APPENDIX
A SOLUTION OF THE WHABA'S PROBLEM

The argument of the minimization can be rewritten as

$$\sum_{i=1}^{k} \left\| b^i - R \cdot b_b^i \right\| = \mathrm{tr}(B^T B) + \mathrm{tr}\left(B_b^T B_b\right) - 2 \cdot \mathrm{tr}\left(R^T B B_b^T\right) \tag{24}$$

where B and B_b are the $3 \times k$ matrix whose columns are the baselines coordinates in the two frames enu and uvw, respectively; tr indicates the trace operator (sum of elements on the main diagonal). Minimizing (23) corresponds to maximizing the last term on the right-hand side of (24). If the product BB_b^T is nonsingular, it can be expressed via the SVD as the product of two orthogonal matrices P_1 and P_2 and a diagonal matrix D. Therefore, the form to maximize is

$$\mathrm{tr}\left(R^T P_1 D P_2^T\right) = \mathrm{tr}\left(P_2^T R^T P_1 D\right) = \sum_{k=1}^{n} x_{ii} d_i \tag{25}$$

where x_{ii} are the diagonal elements of the matrix $X = P_2^T R^T P_1$. Being X a product of orthonormal matrices, all its entries assume values in the interval $[-1; 1]$, and the maximizer of (25) is obtained imposing $\check{X} = I_k$. Since the determinant of $\check{R}$ must be $+1$, the determinant of X ($\det X = \det R \cdot \det(P_2^T P_1)$) must be negative if $\det(P_2^T P_1)$ is negative: therefore the minimizer of (24) is

$$\check{R} = P_1 \check{X} P_2^T, \qquad \text{with } \check{X} = \begin{bmatrix} \det(P_2^T P_1) & 0 \\ 0 & I_{k-1} \end{bmatrix}. \tag{26}$$

ACKNOWLEDGMENT

The authors would like to thank the Hong Kong Marine Department for running the ship trials, as well as A. P. Moller—Maersk for providing access to the ships for the measurements. The authors would also like to thank Dr. C. C. J. M. Tiberius, from the MGP Department, Delft University of Technology (TU Delft), Delft, The Netherlands, for providing assistance with the Schie canal test. The Australian tests were performed during a visiting period that the first author spent at the GNSS Laboratory, Curtin University of Technology, Perth, W.A., Australia. G. Giorgi would like to thank Dr. S. Verhagen, from TU Delft, and the whole Curtin GNSS research group: their support has been invaluable.

REFERENCES

[1] M. Ueno and R. Santerre, "GPS attitude for a berthing guidance system," *Can. Aeronaut. Space J.*, vol. 45, no. 3, pp. 264–269, 1999.
[2] M. Ueno and R. Santerre, "A combined method for GPS ambiguity resolution with single-frequency receivers: Application for ship berthing," *Navigation*, vol. 47, no. 2, pp. 100–111, 2000.
[3] L. P. Fortes, G. Lachapelle, M. E. Cannon, G. Marceau, S. Ryan, S. Wee, and J. Raquet, "Testing of a multi-reference GPS station network for precise 3D positioning in the St. Lawrence Seaway," in *Proc. Int. Tech. Meeting Satellite Div. Inst. Navig.*, Nashville, TN, 1999, pp. 1259–1270.
[4] T. P. Gourlay and K. Klaka, "Full-scale measurements of containership sinkage, trim and roll," *Austral. Naval Architect*, vol. 11, no. 2, pp. 30–36, 2007.
[5] T. P. Gourlay, "Dynamic draught of container ships in shallow water," *Int. J. Maritime Eng.*, vol. 150, no. A4, pp. 43–56, 2008.
[6] E. Desa, P. K. Maurya, A. Pereira, A. M. Pascoal, R. G. Prabhudesai, A. Mascarenhas, E. Desa, R. Madhan, S. G. P. Matondkar, G. Navelkar, S. Prabhudesai, and S. Afzulpurkar, "A small autonomous surface vehicle for ocean color remote sensing," *IEEE J. Ocean. Eng.*, vol. 32, no. 2, pp. 353–364, Apr. 2007.
[7] I. F. Ihle, J. Jouffroy, and T. I. Fossen, "Formation control of marine surface craft: A Lagrangian approach," *IEEE J. Ocean. Eng.*, vol. 31, no. 4, pp. 922–934, Oct. 2006.
[8] G. Lu, G. Lachapelle, M. E. Cannon, and B. Vogel, "Performance analysis of a shipborne gyrocompass with a multi-antenna GPS system," in *Proc. IEEE Position Location Navig. Symp.*, 1994, pp. 337–343.
[9] M. Ueno, "A GPS-based system for precise shipping guidance and control," *J. Mar. Sci. Technol.*, vol. 5, pp. 9–15, 2000.
[10] P. J. G. Teunissen, G. Giorgi, and P. J. Buist, "Testing of a new single-frequency GNSS carrier-phase compass method: Land, ship and aircraft experiments," *GPS Solutions*, vol. 15, no. 1, pp. 15–28, 2010.
[11] R. Lehmann and B. Koop, "Conveyance of large cruise liners—Geodetic investigation of rolling and track prediction," *J. Appl. Geodesy*, vol. 3, no. 3, pp. 131–141, 2009.
[12] D. Kim and R. B. Langley, "GPS ambiguity resolution and validation: Methodologies, trends and issues," in *Proc. 7th GNSS Workshop/Int. Symp. GPS/GNSS*, Seoul, Korea, 2000, pp. 213–221.
[13] P. J. Buist, "The baseline constrained LAMBDA method for single epoch, single frequency attitude determination applications," in *Proc. Int. Tech. Meeting Satellite Div. Inst. Navig.*, Fort Worth, TX, 2007, pp. 2962–2973.
[14] P. J. G. Teunissen, "Integer least squares theory for the GNSS compass," *J. Geodesy*, vol. 84, no. 7, pp. 433–447, 2010.
[15] P. J. G. Teunissen, "Integer least-squares estimation of the GPS phase ambiguities," in *Proc. Int. Symp. Kinematic Syst. Geodesy, Geomatics Navig.*, Banff, AB, Canada, 1994, pp. 221–231.

[16] P. J. G. Teunissen, "The least-squares ambiguity decorrelation adjustment: A method for fast GPS integer ambiguity estimation," *J. Geodesy*, vol. 70, pp. 65–82, 1995.
[17] F. Boon and B. A. C. Ambrosius, "Results of real-time applications of the LAMBDA method in GPS based aircraft landings," in *Proc. Kinematic Syst. Geodesy Geomatics Navig.*, 1997, pp. 339–345.
[18] D. B. Cox and J. D. Brading, "Integration of LAMBDA ambiguity resolution with Kalman filter for relative navigation of spacecraft," *Navigation*, vol. 47, no. 3, pp. 205–210, 2000.
[19] S. Ji, W. Chen, C. Zhao, X. Ding, and Y. Chen, "Single epoch ambiguity resolution for Galileo with the CAR and LAMBDA methods," *GPS Solutions*, vol. 11, pp. 259–268, 2007.
[20] S. Q. Huang, J. X. Wang, X. Y. Wang, and J. P. Chen, "The application of the LAMBDA method in the estimation of the GPS slant wet vapour," *Acta Aeronautica et Astronautica Sinica*, vol. 50, no. 1, pp. 60–68, 2009.
[21] R. Kroes, O. Montenbruck, W. Bertiger, and P. Visser, "Precise GRACE baseline determination using GPS," *GPS Solutions*, vol. 9, pp. 21–31, 2005.
[22] P. J. G. Teunissen and A. Kleusberg, *GPS for Geodesy*. Berlin, Germany: Springer-Verlag, 1998, ch. 5.
[23] G. H. Golub and C. F. V. Loan, *Matrix Computations*. Baltimore, MD: The Johns Hopkins Univ. Press, 1996, ch. 12.
[24] P. J. G. Teunissen, "The LAMBDA method for the GNSS compass," *Artif. Satellites*, vol. 41, no. 3, pp. 89–103, 2007.
[25] G. Giorgi, P. J. G. Teunissen, and P. J. Buist, "A search and shrink approach for the baseline constrained LAMBDA: Experimental results," in *Proc. Int. Symp. GPS/GNSS*, A. Yasuda, Ed., 2008, pp. 797–806.
[26] G. Giorgi and P. J. G. Teunissen, "Carrier phase GNSS attitude determination with the multivariate constrained LAMBDA method," in *Proc. IEEE-AIAA Aerosp. Conf.*, Big Sky, MT, 2010, DOI: 10.1109/AERO.2010.5446910.
[27] C. Park and P. J. G. Teunissen, "A new carrier phase ambiguity estimation for GNSS attitude determination systems," in *Proc. Int. GPS/GNSS Symp.*, Tokyo, Japan, 2003, pp. 249–255.
[28] R. H. Battin, *An Introduction to the Mathematics and Methods of Astrodynamics*, ser. AIAA Education. Reston, VA: AIAA, 1987, ch. 2.
[29] G. Wahba, "Problem 65-1: A least squares estimate of spacecraft attitude," *SIAM Rev.*, vol. 7, no. 3, pp. 384–386, 1965.
[30] T. P. Gourlay, "Ship underkeel clearance in waves," in *Proc. Coasts Ports*, Melbourne, Vic., Australia, 2007.
[31] General Secretariat of the Permanent International Association of Navigation Congresses, "Approach channels: A guide for design," Final Report of the Joint PIANC-IAPH Working Group II-30 in cooperation with IMPA and IALA, Suppl. PIANC Bull. 95, 1997.
[32] Maritime New Zealand, "Accident report: Grounding of Eastern Honor in the approaches to Whangarei on 27 July 2003," [Online]. Available: www.maritimenz.govt.nz
[33] Maritime New Zealand, Accident report: Capella Voyager grounding in the approaches to Whangarei on 16 April 2003 [Online]. Available: www.maritimenz.govt.nz
[34] Maritime New Zealand, "Accident report: Grounding of Jody F Millennium near Port of Gisborne on 6 February 2002," [Online]. Available: www.maritimenz.govt.nz

Gabriele Giorgi received the B.S. degree in aerospace engineering and the M.S. degree in space engineering from University of Rome, Rome, Italy, in 2003 and 2006, respectively, and the Ph.D. degree from the Delft University of Technology, Delft, The Netherlands.

He is a Research Assistant at the Institute for Communications and Navigation, Technische Universität München, Munich, Germany. His main research focuses on ambiguity resolution, attitude determination with next-generation GNSS, and high integrity applications.

Peter J. G. Teunissen (M'10) received the Ph.D. degree in geodesy from Delft University of Technology (DUT), Delft, The Netherlands, in 1985.

He attained full Professorship of Geodesy and Navigation in 1988. He has been Head of Mathematical and Physical Geodesy Department, Faculty of Geodesy (1993–1998); Vice-Dean of Faculty of Civil Engineering & Geosciences (2001–2002); Director of Education (2002–2004); and Head of Earth Observation and Space Systems Department, Faculty of Aerospace Engineering (2003–2006). He is a Federation Fellow of the Australian Research Council (ARC), Professor of Geodesy and Navigation and Leader of the Global Navigation Satellite System (GNSS) research lab, Curtin University of Technology (CUT), Perth, W.A., Australia. His current research focus is on next-generation GNSS for relative navigation and attitude determination for land, maritime, and aerospace applications. He is the inventor of the LAMBDA method and has 25 years of GNSS research experience.

Prof. Teunissen was elected Fellow of the Royal Netherlands Academy of Sciences in 2000 and Fellow of the International Association of Geodesy (IAG) in 1991.

Tim P. Gourlay received the B.Sc. degree from the University of Melbourne, Melbourne, Vic., Australia, in 1993 and the B.App.Maths Hons. and the Ph.D. degree in applied mathematics from University of Adelaide, Australia, in 1994 and 2000, respectively.

He is a Senior Research Fellow with the Centre for Marine Science and Technology, Curtin University of Technology (CUT), Perth, W.A., Australia. He is active in the area of ship under-keel clearance (UKC) research, including performing full-scale measurements of ship sinkage and wave-induced motions using real-time kinematic (RTK) Global Positioning System (GPS).